Transactions of the SMiRT 27
Yokohama, Japan, March 3-8, 2024
Division IV

Statistical Property of Spatial Correlation and Variation of Spectral Ratio with Respect to Common Reference Point Estimated by Dense Seismic Observation at Hard-rock Site

Takanobu Sato[1], Hiroaki Sato[2]

[1] Research Scientist, Central Research Institute of Electric Power Industry, Chiba, Japan (tak-sato@criepi.denken.or.jp)
[2] R&D Manager/Senior Research Scientist, Central Research Institute of Electric Power Industry, Chiba, Japan

ABSTRACT

We conducted a dense seismic observation at a hard-rock site, which is expected to be a certain homogeneity, and assessed the statistical property of the spatial correlation. This was based on the relationship between cross-correlation coefficients and the distance of observation station pairs, utilizing the seismic records obtained. The spatial correlation was modeled using the lower limit of the correlation coefficients a and the spatial distance b and evaluated in four areas within the target site. As a result of the evaluation of the spatial correlation at multiple center frequencies, it was shown that the spatial correlations in each area were almost the same. In a detailed confirmation, the correlation distances b for each area were estimated almost identical as a result of the calculation to reduce the effect of a trade-off between parameters a and b. The similarity of the correlation distance b for each area indicates that the horizontal homogeneity of each area is similar, which is believed to reflect the similar stratification of the velocity structure. Then, we calculated the S-wave spectral ratios of the observation station pairs and evaluated their variation for each earthquake using the standard deviation. The standard deviations of the S-wave spectral ratios tended to increase with increasing frequency, which is the opposite trend of the correlation coefficient. We regressed their characteristics for frequency in four areas, respectively, and compared them. As a result, the regressed characteristics of standard deviations were almost the same in each area.

INTRODUCTION

The velocity structure models used for earthquake ground motion evaluation at critical facility sites are often constructed using 1-D models based on geological surveys and geophysical exploration. Therefore, it is important to check the validity of the one-dimensional approximation of the structure within the entire site during modeling. Previous studies have reported that peculiar ground motion amplifications were observed for ground motions arriving from a specific area within a site or a specific direction (e.g. Sato and Torii (2019)). Therefore, a thorough investigation of the azimuthal dependence of ground-motion amplification within a site is an effective approach to assess whether local velocity structural changes impact site amplification. However, it is difficult to obtain sufficient seismic records for observation record analysis in low-seismicity regions. Even when seismic records can be obtained, the epicentral direction is often biased. Therefore, it is difficult to apply this method to multiple sites.

In this study, we explored a method to assess the validity of a one-dimensional approximation in velocity structure modeling, independent of the earthquake dataset, using seismic records obtained from a dense seismic observation at hard-rock sites. The validity of the one-dimensional approximation has been previously assessed. Torii et al. (2021) investigated the similarity of spatial correlations estimated for four areas within the site using seismic records with JMA magnitude (Mj) 2.0 or higher and hypocenter depth 100 km or shallower. Sawada et al. (2019) investigated the variation in S-wave spectral ratios for each earthquake, utilizing seismic records with hypocenter distance 600 km or shorter. They indicated that this

variation was attributed to uncertainty in ground motion amplification. These studies, with earthquake selection criteria not being severe are deemed applicable to low-seismicity regions and are considered effective for assessing the validity of the one-dimensional approximation. Hence, we evaluated the spatial correlation and standard deviation of S-wave spectral ratios, indicative of the subsurface velocity structure, employing seismic records from a dense seismic observation at the target site. Specifically, we established a model for the relationship between cross-correlation coefficients and distances among observation station pairs in four areas within the target site. Subsequently, we analyzed the parameters to assess the one-dimensional approximation's validity based on their congruence. In addition, we calculated the regression of the standard deviation of the S-wave spectral ratios and frequency using a common reference point and area and evaluated the characteristics.

DENSE SEISMIC OBSERVATION AND SEISMIC RECORD

We conducted a dense seismic observation at the hard-rock site, which was expected to have a certain homogeneity. This site has been confirmed to exist on hard rock ground, and the S-wave velocity is approximately 2.2 km/sec based on the PS logging of the boring data. Seismic observations were conducted at nine stations on the ground surface at the target site, covering an area approximately 1 km in diameter, as shown in Figure 1. The first period was from June 12, 2019, to December 18, 2019, and the second period was from June 24, 2020, to May 30, 2023. In the first period, there were seven observation stations (No. 1 to No. 7), and in the second period, Nos.8 and 9 were added to the existing seven stations to increase spatial density.

The seismic records were selected based on the unified hypocenter list by the Japan Meteorological Agency, and that were Mj 2.0 or higher, epicenter distance 200 km or shorter, and hypocenter depth 100 km or shallower. An S/N ratio below a factor of three was eliminated from subsequent analyses. Figure 2 shows the epicenter distribution map of the 369 earthquakes that satisfied the above conditions.

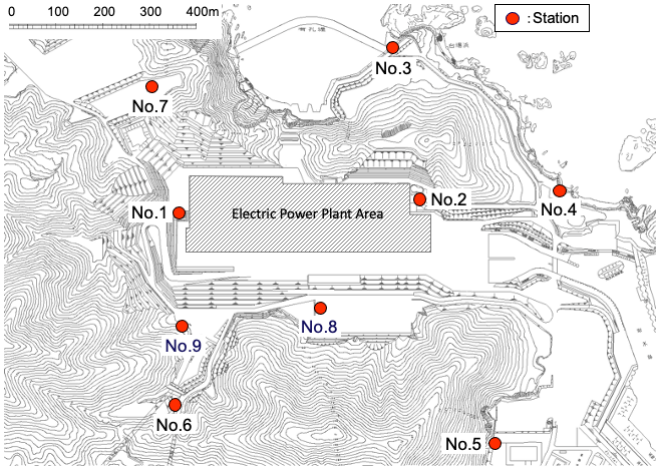

Figure 1. Distribution of observation stations at target site.

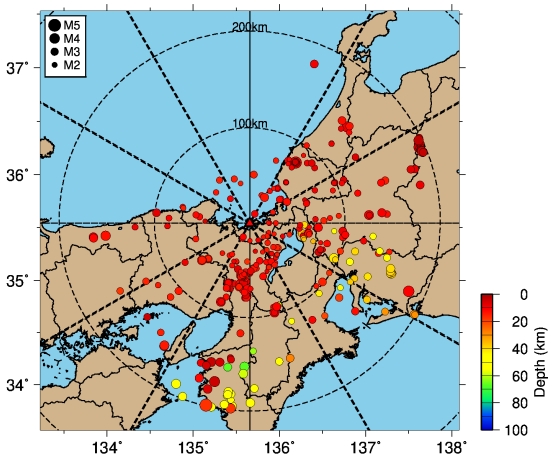

Figure 2. Distribution of epicenters of the obtained earthquakes.

STATISTICAL PROPERTY OF SPATIAL CORRELATION

Cross-Correlation Coefficient

Spatial variations in earthquake ground motion between observation station pairs were evaluated via a cross-correlation analysis using the S-wave portion. First, a primary cut-out of the entire seismic wave from

the continuous record was performed based on the event list. Next, we picked out the S-wave portion and applied a narrow bandpass filter for center frequencies of 1.5, 1.9, 2.4, 3.0, 3.8, 4.8, 6.0, 7.6, 9.5, and 12.0 Hz with a 1/3 octave-band width. Finally, a secondary cut-out of the S-wave portion for 3.4 sec was performed for each of the two horizontal components. However, a frequency lower than 1.5 Hz was excluded from this study because a decrease in S/N was suspected based on the confirmation of the S-wave Fourier spectrum.

The cross-correlation coefficients were computed using the bandpass-filtered S-wave time history for every station pair at an interval of 0.01 sec using Equation (1).

$$cor\left(r_{ij}, \delta t; f\right) = \frac{\int w_i(t;f) w_j(t+\delta t;f) dt}{\sqrt{\int w_i^2(t;f) dt \int w_j^2(t;f) dt}} \quad (1)$$

where r_{ij} is the distance of station pair i and j, and δt is the lag time. $w_i(t;f)$ is the bandpass-filtered (center frequency f) S-wave time history at station i. Finally, we choose the maximum cross-correlation coefficient, which we call the cross-correlation coefficient $cor\left(r_{ij};f\right)$. Thus, the cross-correlation coefficients of every station pair for every earthquake were obtained for each center frequency. S-wave time histories were used for both the NS and EW components, and cross-correlation coefficients were computed for each component. In the cross-correlation analysis, it is necessary to avoid the influence of observation station-specific shallow underground structures. Therefore, if an obvious peak was identified in the microtremor H/V spectrum of a station, we only used cross-correlation coefficients whose center frequency was lower than the peak frequency for the station pairs that included that station. The cross-correlation coefficients obtained for each station pair were not constant and varied with the earthquake. Torii et al. (2021) utilized a log-normal distribution to model the cumulative relative frequency distribution of cross-correlation coefficients obtained for each station pair. They adopted the median value of the log-normal distribution as the representative value for the station pair. The cross-correlation coefficients obtained in this study were also well-modeled. Therefore, we adopted the median value of the log-normal distribution as the representative value of the station pair.

Spatial Correlation

The spatial correlation within the site, derived from a dense seismic observation, was estimated by analyzing the relationship between the distances among station pairs and cross-correlation coefficients. Figure 3 shows the relationship between the distances and cross-correlation coefficients for each center frequency. The cross-correlation coefficients initially decrease with increasing distance and finally asymptote to a certain value. Note that at higher frequencies, the amount of data was reduced because some data was removed based on the relationship between the center frequency and peak frequency of the microtremor H/V spectrum. Because the relationship between the cross-correlation coefficients and the distances of station pairs in this study showed the same trend as the model of Horike and Takeuchi (2000), we used the same spatial correlation model $c_f(r)$ as the function of Equation (2) for fitting to estimate the statistical properties.

$$c_f(r) = a + (1-a)\exp\left(-\frac{r}{b}\right) \quad (2)$$

where r is the distance between station pairs, a is the lower limit of the correlation coefficients, and b (m) is the parameter controlling the shape of the regression curve, which corresponds to the correlation distance. The values of regression parameters a and b were computed using simulated annealing (Torii et al. (2021)). Figure 3 also shows the modeling results of the spatial correlations using Equation (2) for each center frequency, all of which are well modeled. In addition, the regression results for parameters a

and b are presented. We found that the identified parameter a was at a maximum at a center frequency of 1.5 Hz and decreased with increasing center frequency, reaching a minimum at 12 Hz. In addition, the identified parameter b decreased with increasing center frequency up to 6 Hz and finally converged at approximately 100 m. It was expected that the longer the correlation distance, the higher the spatial homogeneity. At present, however, it is not possible to determine the degree of spatial homogeneity based on the magnitude of the correlation distance. It is expected that similar studies will be conducted at multiple sites in the future. At the same time, the results will be compared with the geological structure, and the correlation distance will become one of the standard values indicating homogeneity.

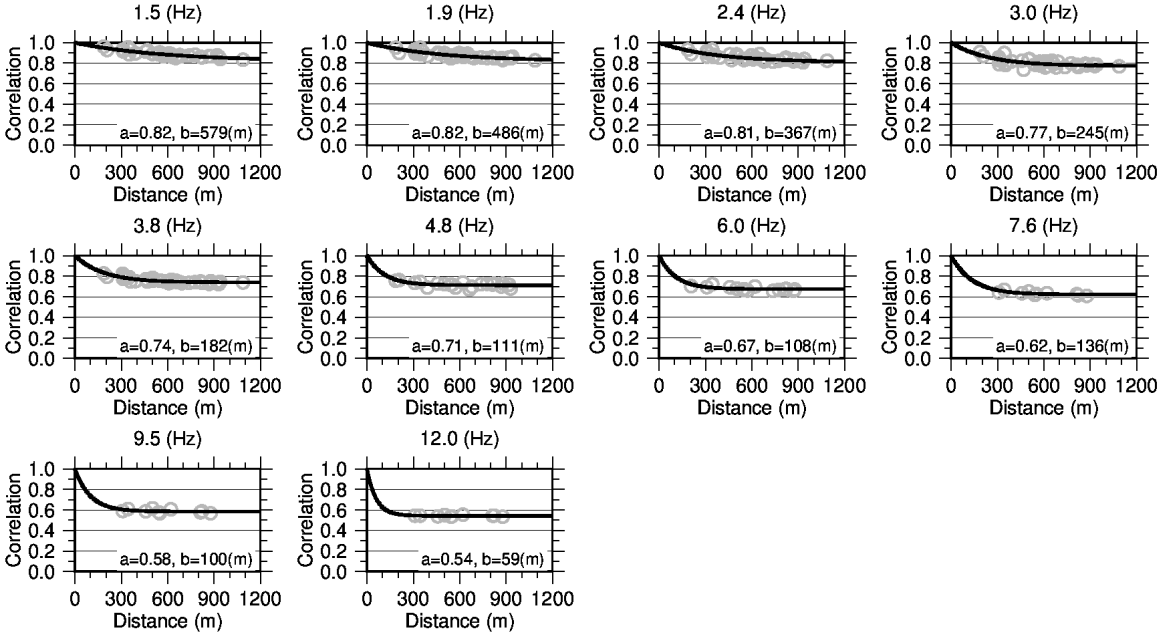

Figure 3. Spatial correlation obtained using all stations for each center frequency. The circles represent the relationship between the representative values of the cross-correlation coefficients and distance for each station pair. The solid lines represent the regression results by using Equation (2).

Spatial Correlation for Each Area

If the distance attenuation characteristics of the cross-correlation coefficients or spatial correlation are attributable to the subsurface velocity structure of the site, then the spatial correlation obtained using all observation stations at the site is considered to reflect the characteristics of the subsurface velocity structure for the site. However, the local spatial correlation within a site reflects the characteristics of the local subsurface velocity structure. Therefore, by estimating multiple local spatial correlation within the site, there is a possibility that the similarity of the spatial correlation may represent the spatial similarity of the subsurface velocity structure and consequently assess of the validity of the one-dimensional approximation. In this section, we divide the site into four areas: areas A (northeast side), B (southwest side), C (northwest side), and D (southeast side), as shown in Figure 4(a), and estimate the spatial correlations for each area. Each area contained six stations, and the stations near the boundaries overlapped. Figure 4(b) shows the results of the spatial correlations for each area, which were estimated using only station pairs within each area. By comparing the spatial correlations of each area in the figure, we found that the spatial correlations of each area were almost the same. We excluded the results for center frequencies above 6 Hz because some areas could not be modeled due to data removal considering the peak frequency of the microtremor H/V spectrum.

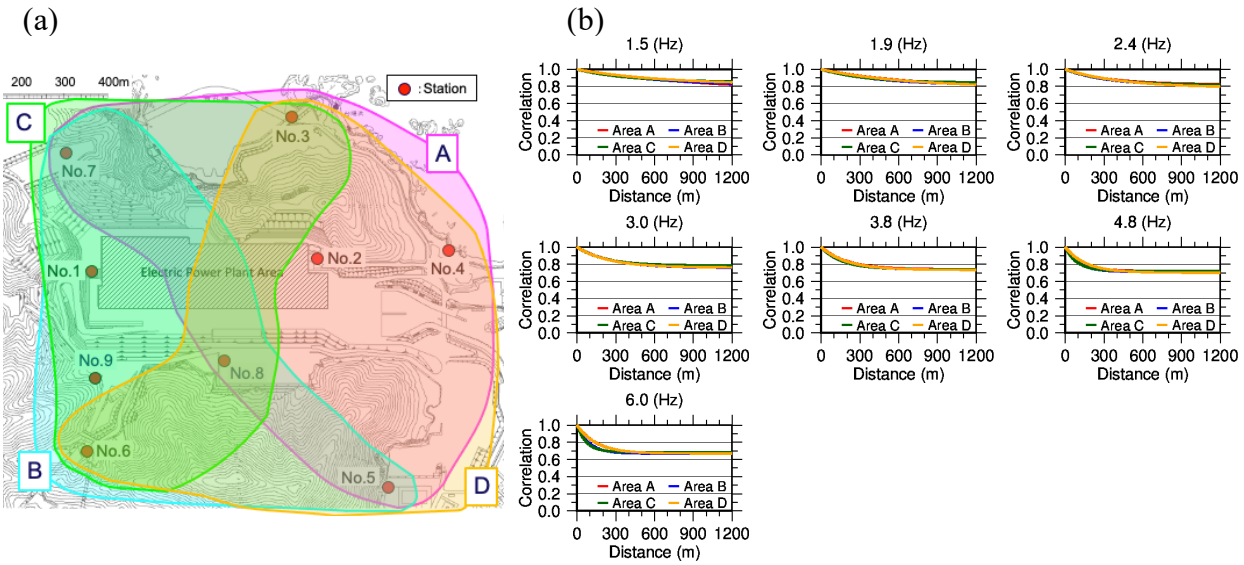

Figure 4. (a) Observation station and area division at the target site. (b) Comparison of regression results of spatial correlations in each area for each center frequency. Center frequencies above 6 Hz were excluded because some area could not be modeled.

For detailed confirmation, the lower limit of the correlation coefficients a and the correlation distance b estimated by modeling the spatial correlation were compared between the areas. Figure 5(a) shows a comparison of the lower limit of the correlation coefficients a with respect to the center frequency between areas, and the parameters a are in good agreement for all areas above 2 Hz. In addition, Figure 5(b) shows a comparison of the correlation distance b with respect to the center frequency between areas. Parameter b are good agreement for all areas above 2 Hz, similar to parameter a. It was found that the variations at the lower frequency were greater for parameter b than for parameter a. Because the lower limit of the correlation coefficient for frequencies lower than 2 Hz is not flat and is unclear, it is possible that a trade-off between parameters a and b is more likely to occur. Figure 5 also shows the results obtained using all stations, which plot within the medium magnitude of the results for each area.

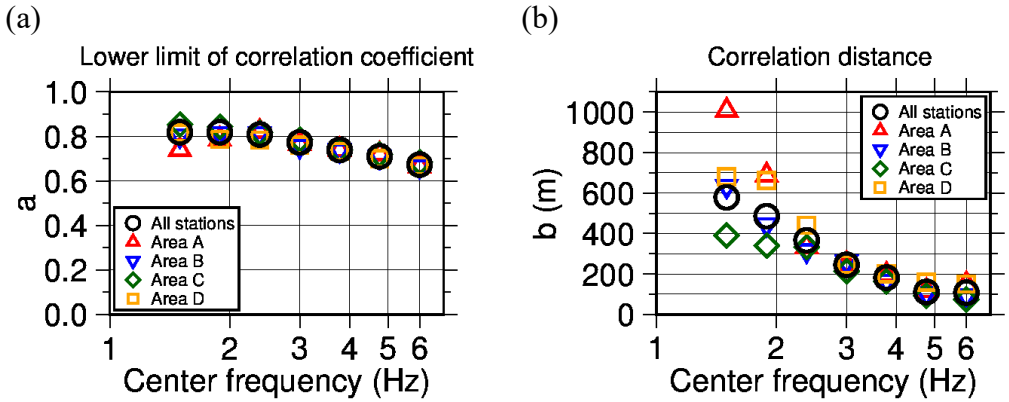

Figure 5. (a) Relationship between center frequency and lower limit of correlation coefficient a in each area. (b) Relationship between center frequency and correlation distance b in each area. Parameters a and b estimated by using all stations are also shown. Center frequencies above 6 Hz were excluded because some area could not be modeled.

As mentioned above, the correlation distance b is an important indicator of the scale of the horizontal homogeneity. However, it is possible that the parameters a and b in Figure 5 could not be estimated correctly due to the effect of a trade-off. Since the target site is a hard-rock site that is expected to be a certain homogeneity, it is expected that the spatial correlations estimated for each area are generally consistent. Therefore, to reduce the effect of a trade-off between parameters a and b, we fixed the parameter a obtained using all stations and estimated the parameter b of the spatial correlations for each area. Figure 6 shows a comparison of the parameter b with respect to the center frequency between areas, and the parameters b are in good agreement for all areas. Also, it was found that the parameters b estimated in each area were almost the same as the ones obtained using all stations shown in Figure 5. The similarity of the correlation distance b for each area indicates that the horizontal homogeneity of each area is similar, which is believed to reflect the similar stratification of the velocity structure.

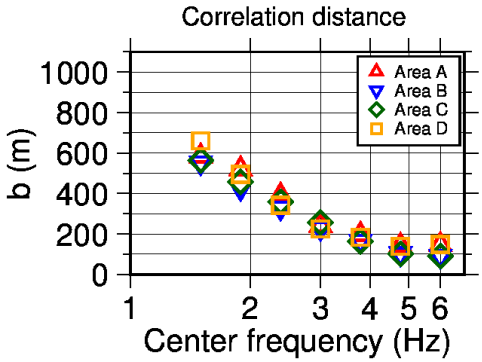

Figure 6. Relationship between center frequency and correlation distance b in each area. In regression, parameter a was fixed using the result obtained using all stations. Center frequencies above 6 Hz were excluded because some area could not be modeled.

VARIATION OF S-WAVE SPECTRAL RATIO WITH COMMON REFERENCE POINT

S-wave spectral ratios and standard deviation with common reference point

For spatial variations in earthquake ground motions at a hard-rock site, Sawada et al. (2019) examined the variations in the S-wave spectral ratios from each earthquake using dense seismic observation records, and they indicated that the variations were due to uncertainty in ground motion amplification. If the variations in the S-wave spectral ratios are attributable to the subsurface velocity structure of the site, they may be used to discuss the spatial homogeneity of the subsurface velocity structure, similar to the spatial correlation. Therefore, we calculated S-wave spectral ratios using dense seismic observation records at the target site and evaluated their variations using standard deviations. For the spectral analysis, we used the S-wave portion of the two horizontal components. First, a primary cut-out of the entire seismic wave from a continuously recorded wave is performed based on the event list. Next, we applied a 1-10 Hz bandpass filter and performed a secondary cut-out of the S-wave portion for 20.48 sec. Finally, we executed a Fast Fourier Transform (FFT) and calculated the smoothed spectrum using a Parzen window of 0.5 Hz. The S-wave spectral ratio was estimated by dividing the Fourier spectrum of one station by that of another station for the same earthquake. For each station pair, the S-wave spectral ratios for each earthquake were calculated, and the mean and standard deviation for each frequency were obtained. As an example, the S-wave spectral ratios and their means for all earthquakes are shown in Figure 7(a) and 7(c) for station No.2 and No.3 pairs and No.2 and No.7 pairs, respectively. The standard deviations of the S-wave spectral ratios are shown in Figure 7(b) and 7(d). From the figure, it can be observed that the standard deviation increases with increasing frequency on a logarithmic scale. Therefore, we calculated the regression of the standard deviation, SD and frequency, f (Hz), using Equation (3), to evaluate its characteristics.

$$SD = mlog(f) + n \quad (3)$$

where m and n are the regression parameters. Figure 7(b) and 7(d) show the regression results.

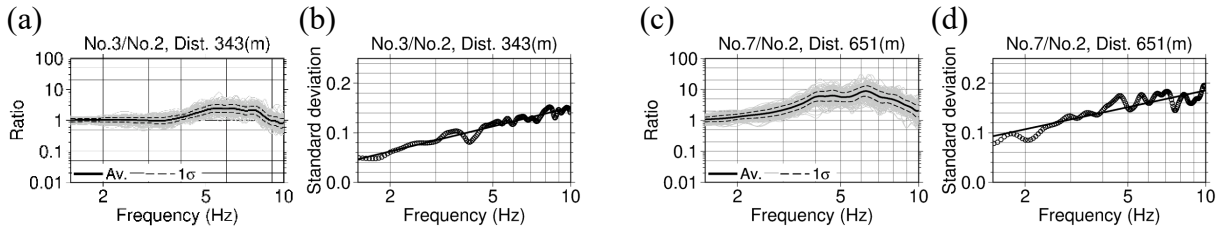

Figure 7. (a) S-wave spectral ratios and average spectra of the No.2 and No.3 pairs. (b) Standard deviation of S-wave spectral ratios of No.2 and No.3 pairs. (c) S-wave spectral ratios and average spectra of the No.2 and No.7 pairs. (d) Standard deviation of S-wave spectral ratios of No.2 and No.7 pairs.

To confirm the characteristics of each station used to calculate the S-wave spectral ratio, we evaluated each station from No.1 to No.9 as a common reference point. Specifically, the standard deviations of the S-wave spectral ratios were calculated for station pairs, including the reference points. Figure 8(a) shows the regression results of the standard deviation using Equation (3) when Nos. 1–9 were used as the reference points, with the color corresponding to the distance between the reference point and each station. The average standard deviation, shown as a solid line in the figure, is the regression result obtained using the average standard deviation of each station pair for each frequency. The relationship between the standard deviations of the S-wave spectral ratios and the distances between station pairs showed that the standard deviation tended to increase with increasing distance. As discussed in the previous section, the cross-correlation coefficient tends to decrease with increasing distance. This suggests that the standard deviation of the S-wave spectral ratios and the cross-correlation coefficient may have opposite characteristics

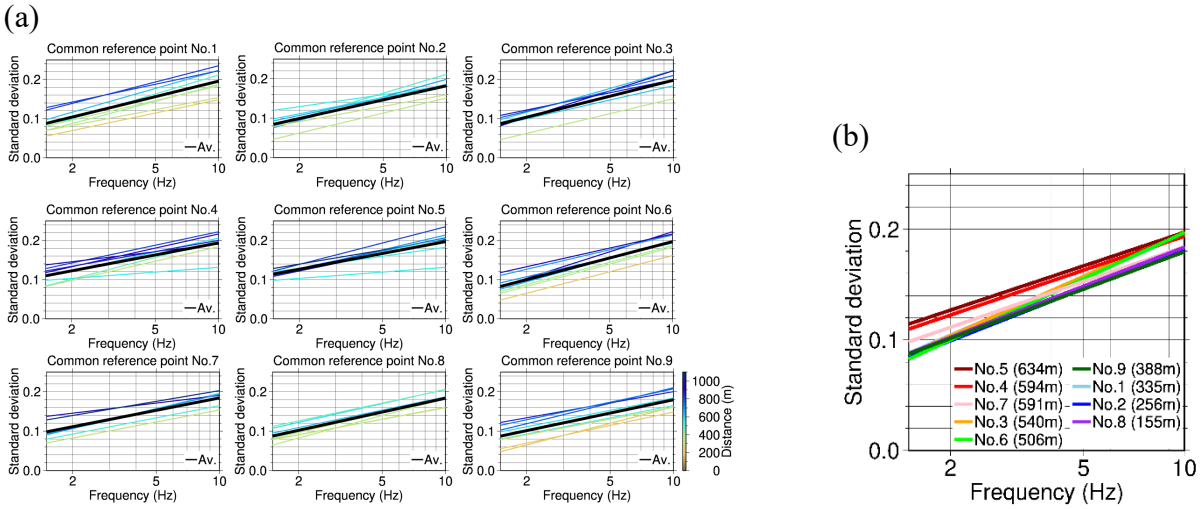

Figure 8. (a) Regression results of the standard deviation of S-wave spectral ratios and the average standard deviation for each reference point. The color scale denotes the distance between the reference point and each station. (b) Comparison of the average standard deviation of each reference point. The distances between the reference point and the centroid of the other stations are described.

concerning distance. Figure 8(b) shows a comparison of the average standard deviations for reference points No. 1 to No. 9, with colors corresponding to the reference point. The distances shown in the figure were the result of determining the distance between the reference point and the centroid of the other stations to evaluate the relationship between the location of the reference point and the distribution of the observation stations. The figure shows that the standard deviations were large for Nos. 4 and 5, where the distances were long, whereas they were small for Nos. 1, 2, 8, and 9, where the distances were short. In addition, Nos. 3, 6, and 7 fall within the medium range of standard deviations and distances. These results indicate that the magnitude of the standard deviation corresponds to the magnitude of the distance. However, in the short-distance group, the standard deviations were almost the same in all frequency bands, although there was a difference of more than 200 m from 155m in No.8 to 388 m in No. 9. Therefore, it is inferred that the magnitude of the standard deviation does not generally decrease with decreasing distance, and does not decrease below a certain value.

Standard deviations of S-wave spectral ratios for each area

For the spatial correlation analysis, we divided the target site into four areas and compared the characteristics of the spatial correlations for each area. The standard deviations of the S-wave spectral ratios for each area, shown in Figure 9(a), were evaluated. Specifically, the standard deviations of the S-wave spectral ratios were calculated using only station pairs within each area. Figure 9(b) shows the regression results of the standard deviation for each area, with the color corresponding to the distance between observation station pairs. The average standard deviation, shown as a solid line in the figure, is the regression result obtained using the average standard deviation of each station pair for each frequency. Figure 9(c) compares the average standard deviations for each area. The distances shown in the figure are the result of determining the average distance between the centroids of all stations and each station using only the stations within the area. The figure shows that the standard deviations were almost the same, regardless of the area. The average distance between the centroid and each station was approximately equal for each area, with the smallest being 318 m in Area C and the largest being 368 m in Area A. However, there was a slight variation in standard deviations at lower frequencies, and it was found that the magnitude of the standard deviation corresponded to the magnitude of the distance. It is possible that the effect of the distance was slightly reflected in the standard deviation.

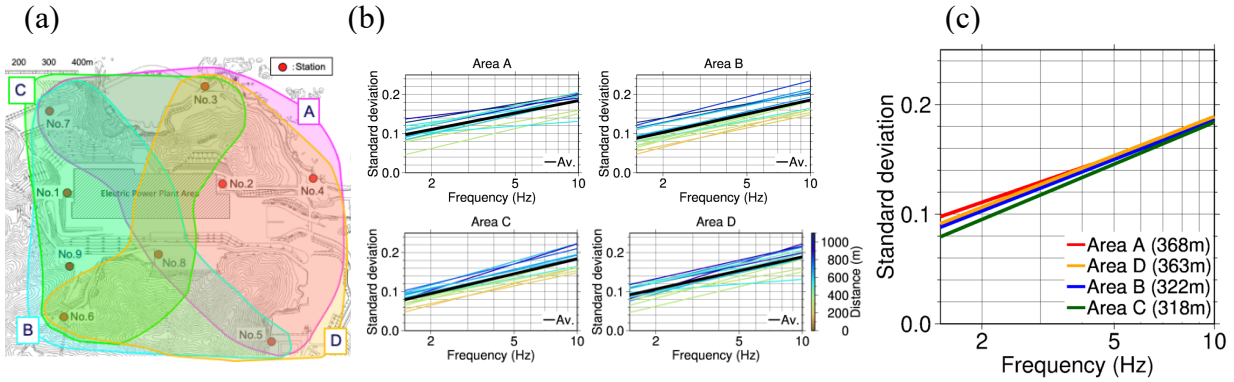

Figure 9. (a) Observation station and area division at the target site. (b) Regression results of standard deviation of S-wave spectral ratios and the average standard deviation for each area. The color scale denotes the distance between observation station pairs. (c) Comparison of the average standard deviation for each area. The average distances between the centroid of all stations and each station only using the stations within the area are described.

CONCLUSION

Using S-wave records of 369 earthquakes obtained from a dense seismic observation at hard-rock sites, we evaluated the statistical properties of spatial correlations based on the relationship between cross-correlation coefficients and distances between observation station pairs. Spatial correlations in multiple center frequencies were estimated for four areas within the site, which were modeled by using the lower limit of correlation coefficients a and the correlation distance b. To reduce the effect of a trade-off between parameters a and b, we modeled with the parameters a fixed to the results obtained using all stations, and the correlation distances b for each area were estimated almost identical. The similarity of the correlation distance b for each area indicates that the horizontal homogeneity of each area is similar, which is believed to reflect the similar stratification of the velocity structure. Next, we calculated the S-wave spectral ratios of the station pairs and evaluated their variations after each earthquake using the standard deviation. The standard deviations of the S-wave spectral ratios tended to increase with increasing frequency, which is the opposite trend of the correlation coefficient. The magnitude of the standard deviation was approximately consistent with the distance between the reference point and the centroid of the other stations, as observed by comparing the average standard deviations of the S-wave spectral ratios for each reference point. In addition, comparing the average standard deviation for each area, the standard deviations were almost the same regardless of the area. However, there is a slight variation in the standard deviation at lower frequencies, and the magnitude of the standard deviation corresponds to the magnitude of the distance.

ACKNOWLEDGMENT

We are grateful to everyone involved with the Kansai Electric Power Company for their helpful arrangements in installing and maintaining the seismic observation stations. We would like to thank the Japan Meteorological Agency (JMA) for providing hypocenter information. We used the Generic Mapping Tools (Wessel and Smith (1998)) for drawing the figures.

REFERENCES

Horike, M. and Takeuchi, Y. (2000). “Possibility of Spatial Variation of High-Frequency Seismic Motions due to Random-Velocity Fluctuation of Sediments,” *Bull. Seismol. Soc. Am.*, USA, 90 1 48-65.

Sato, H. and Torii, D. (2019). “Current status and future scope of underground velocity structure modeling for design basis ground motion at nuclear power plants,” *Central Research Institute of Electric Power Industry Report*, O19002, JP.

Sawada, Y., Tazawa, Y. and Yajima, H. (2019). “Investigation of Uncertainty of Seismic Amplification Characteristics Based on High Density Seismic Observation at Nuclear Sites,” *Proceedings of the 141st SEGJ Conference*, JP.

Torii, D., Sato, H., Higashi, S and Kuriyama, M. (2020). “Investigation of Ground Amplification Characteristics and Its Variation using Seismic Motions and Microtremors Based on Horizontal Array Observation at Hard Rock Site,” *Proceedings of the 143rd SEGJ Conference*, JP.

Torii, D., Sato, H., Yamamoto, S. and Okazaki, A. (2021). “Assessment of the Validity of the One-Dimensional Approximation in the Velocity Structure Modeling Based on the Spatial Correlation of Seismic Motions,” *Proceedings of the 14th SEGJ International Symnal Symposium*, JP.

Wessel, P. and Smith, W. H. F. (1998). “New, improved version of generic mapping tools released,” *EOS Trans. AGU*, USA, 79, 47, 579.